Spatial Orientation And Distribution Of Reservoir Fractures From Scattered Seismic Energy

Mark Willis, Rama Rao, Daniel Burns, Joongmoo Byun,
Earth Resources Laboratory,
Dept. of Earth, Atmospheric and Planetary Sciences
Massachusetts Institute of Technology
Cambridge, MA 02139

Laura Vetri
ENI E&P, Agip
Milan, Italy

Abstract

Expanded details and additional results are presented using a new method (Willis et al, 2003) for determining the reflection and scattering characteristics of seismic energy from subsurface fractured formations. The method is based upon observations made from 3D finite difference modeling of the reflected and scattered seismic energy over discrete systems of vertical fractures. Regularly spaced, discrete vertical fractures impart a ringing coda type signature to any seismic energy which is transmitted through or reflected off of them. This signature varies in amplitude and coherence as a function of several parameters including: 1) the difference in angle between the orientation of the fractures and the acquisition direction, 2) the fracture spacing, 3) the wavelength of the illuminating seismic energy, and 4) the compliance, or stiffness, of the fractures. This coda energy is greatest when the acquisition direction is parallel to the fractures, the seismic wavelengths are tuned to the fracture spacing, and when the fractures have low stiffness. The method uses surface seismic reflection traces to derive a transfer function which quantifies the change in an apparent source wavelet propagating through a fractured interval. The transfer function for an interval with low scattering will be more spike-like and temporally compact. The transfer function for an interval with high scattering will ring and be less temporally compact. When a 3D survey is acquired with a full range of azimuths, the variation in the derived transfer functions allows the identification of subsurface areas with high fracturing and the orientation (or strike) of those fractures. The method was calibrated with model data and then applied to a field with a fractured reservoir giving results which agree with known field measurements.

1. Introduction

The way in which fractures in rock formations affect the seismic waves propagating through them depends on the fractures' mechanical parameters, such as compliance and saturating fluid, and on their geometric properties, such as dimensions and spacing. If the fractures and fracture spacing are small relative to the seismic wavelength, then the fractures cause the reservoir rock to behave like an equivalent anisotropic medium with a symmetry axis normal to the strike of the 'open' fractures. Resulting seismic reflections from the top and bottom of a fractured reservoir will display amplitude variations with offset and azimuth (AVOA) (e.g., Lynn et al., 1996). If the fractures and fracture spacing are close in size to the seismic wavelength, then the fractures will scatter the seismic energy causing a complex seismic signature or coda. This seismic signature will vary as a function of the orientation of the seismic acquisition relative to the fracture orientation. The scattered seismic energy not only provides information about the fracture orientation, but can also be analyzed to provide information about the fracture spacing and fracture density. Observations by previous researchers have demonstrated that scattering effects are sensitive to fracture density in field data as well as numerical and laboratory experiments (e.g., Ata and Michelena, 1995).

Willis et al (2003) presented the concept of this method based mostly upon the analysis of synthetic data from a simple three layer model. The method was shown to indeed be able to detect fracturing from by isolating a single reflection event above and one below an interval of interest. The method was also applied to super gathers about four wells in the Emilio oil field. In this paper we expand the analysis to demonstrate its effectiveness on the five layer model under a more comprehensive set of fracturing situations. This demonstration is critical to the success of the method since field data certainly does not contain isolated events. In addition to analyzing model data, the method is applied to the Emilio field data on a single interval representing the reservoir level across a significant portion of the field.

2. Modeling

We used the 3-D elastic finite difference code developed by Lawrence Berkeley National Laboratory (Nihei et al., 2002) to model a simple reservoir geometry consisting of five horizontal layers as shown in Figure 1. All the layers except the third layer, are homogeneous and isotropic elastic media. The model parameters are given in Table 1. The third layer is 200-m thick and contains parallel, vertical fractures which are as tall as the layer, one grid cell thick (5m) and run the entire width of the model. We generated a series of models with the following fracture spacings: no fractures, 10m, 25m, 35m, 50m, 100m, and 35m Gaussian distribution. We created another model with at 35m spacing in the y direction and 100m at 45 degrees. All models use a 40Hz Ricker wavelet as the seismic source. The receiver spacing is 5m in both the inline and cross line directions.

Table 1. Parameters for model

Layer	Thickness (m)	Vp (m/s)	Vs (m/s)	Density (g/cc)
1	200	3000	1765	2.2
2	200	3500	2060	2.25
3	200	4000	2353	2.3
4	200	3500	2060	2.25
5	200	4000	2353	2.3

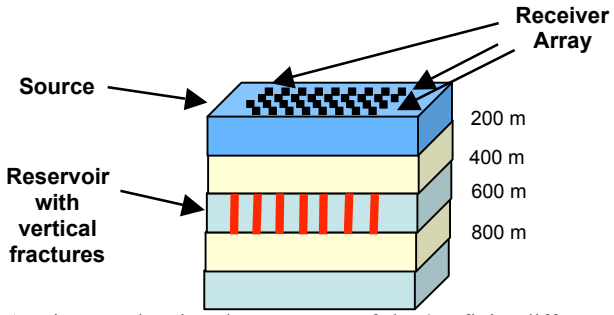

Figure 1. Diagram showing the geometry of the 3D finite difference model. The layer velocities and densities are shown in Table 1. The source is located in the left front corner (red symbol) and the receivers are spread out in a rectangular area 1000 m in the x direction and 1000m in the y direction. The receiver spacing is 5m in each direction.

On the left side of Figure 2 are the shot records for the 50m fracture spacing case acquired in directions normal and parallel to the fractures. To the right of each shot record is its velocity analysis. It is clear on the shot record normal to the fracture direction that there is no coherent stackable energy in or below the reservoir level (300 ms). However, for the parallel case, there are many coherent events that can be seen primarily below the base reservoir reflection on the shot record and observed on the velocity analysis. In the direction parallel to the fractures, the seismic energy seems to be guided by the aligned fractures and the resulting scattered energy is more coherent and similar to the direct P wave reflection. This same pattern of azimuthal variation in the modeled scattered wavefields is observed for all the model results.

For shot records acquired parallel to the fractures, the coherent, ringing scattered events are seen across the near to mid offset ranges. Figure 3 shows the results of applying NMO and stacking the model traces in different azimuthal directions. The trace labeled "normal" corresponds to the stack of the traces in the top left plot of Fig. 2.

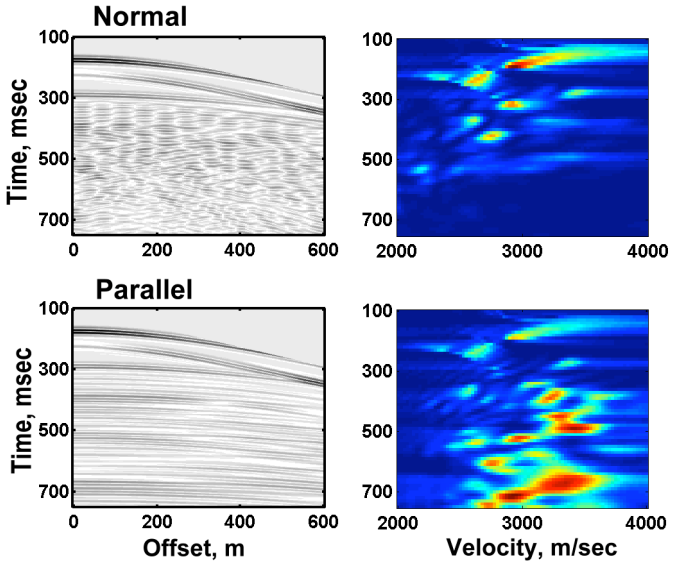

Figure 2: Left two plots show the seismic shot records for the model with 50m fracture spacing. The top left plot show the shot record normal to fractures, left bottom plot shows the shot record parallel to the fractures. The right two plots show the velocity spectra for the corresponding shot records on the left.

The trace labeled "parallel" corresponds to the stack of traces in the bottom left plot of Fig 2. In between these two traces are those stacked traces corresponding to 10 degree increments between normal and parallel directions to the fractures. (For comparison, the bottom trace labeled "control" is the trace from the model with no fractures.) For shot records acquired normal to the fracture direction, the observed scattered wavefield is greatly disruptive with significant back scattered, diffraction-like events. These traces do not stack together well with any NMO velocity. From these observations, the strike of the fracturing may be determined by identifying the azimuthal acquisition direction with shot records containing coherent, ringing energy which are enhanced the most when stacked.

3. Methodology for Stacking and Transfer Functions

In the finite difference model data we generated, it might be possible to directly measure the scattered wavefield from the isolated reflectors in the reservoir zone. However, in field data we expect to have a more difficult time observing these scattered wavetrains due to the nearly continuous nature of the subsurface reflectivity. In addition, if there are fractured zones or other scatterers in the overburden, those scattered waves will contaminate,

or overprint, the scattered energy from our zone of interest in the reservoir. So we start with the concepts from existing methods of seismic wavelet estimation to obtain two apparent (or temporally local) source wavelets from the reflection time series – one from above the fractured zone (the "input" wavelet) and one below it (the "output" wavelet). These wavelets are represented by their autocorrelations obtained from windowed portions of the reflection time series above and below the fractured zone of interest.

We then compute the time domain transfer function between the autocorrelations of the two extracted wavelets. The transfer function is computed by deconvolving the autocorrelation of the input wavelet from the autocorrelation of the output wavelet. This transfer function characterizes the effect of scattering in the interval of interest, between the two windowed portions of the trace. A simple pulse shaped transfer function indicates no scattering, while a long ringing transfer function captures the scattering within the reservoir interval. Notice that any contamination from scattering above the interval will be present in both the input and output extracted wavelets and thus will be excluded from the transfer function.

This method can be used on both pre-stack and post-stacked data. If it is applied to data stacked in different azimuthal directions, the interval transfer function should exhibit greater ringing in the direction parallel to fracturing. Figure 4 shows the transfer functions derived for the stacked traces in Figure 3.

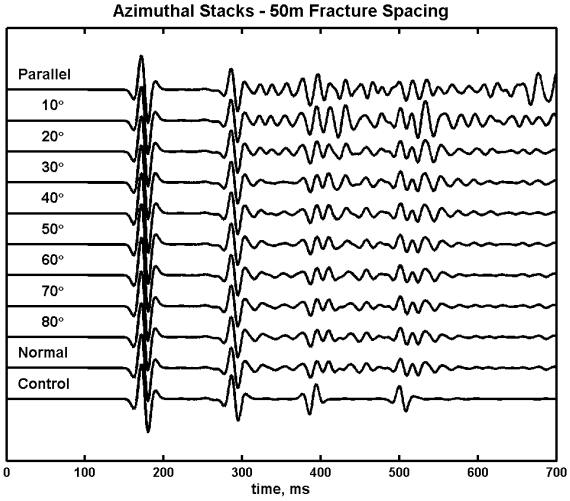

Figure 3: Plot showing the azimuthal stacks of traces from the 50m fracture spacing model. The traces represent azimuth stacks starting in the direction parallel to fracturing (top), and then increasing in 10 degree increments until normal to the fractures. The bottom trace shows the stack for the model without a fractured layer.

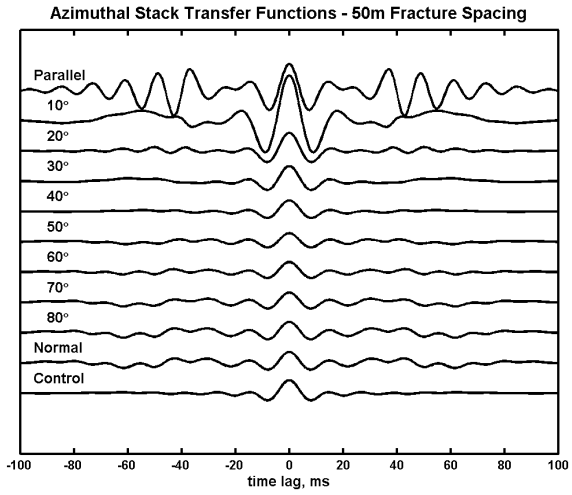

Figure 4: Plot showing the transfer functions corresponding to azimuthal stacks of traces (in Fig. 3) from the 50m fracture spacing model. The transfer functions correspond to azimuth starting in the direction parallel to fracturing (top), and then increasing in 10 degree increments until normal to the fractures. The bottom trace shows the transfer function for the model without a fractured layer.

One of the first questions to be answered is whether this methodology is applicable for fracture systems which are not perfectly regular or have multiple sets of fractures. We generated additional models to address these questions. Figure 5 shows the azimuthal stacks for the 35m fracture case and Figure 6 shows the corresponding transfer functions.

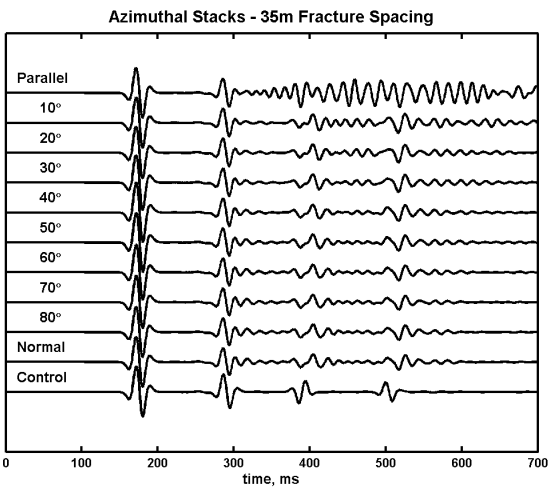

Figure 5. Azimuthal stacks for 35m fractures.

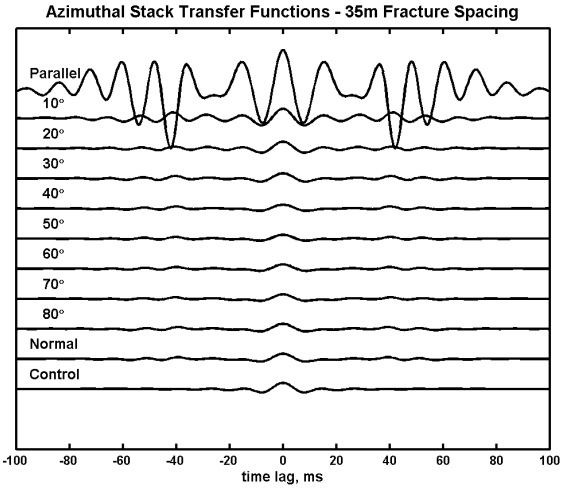

Figure 6. Transfer functions for 35m fractures stacks.

We next varied the spacing of the fractures to have a Gaussian distribution about 35m and standard deviation of 10m. Figures 7 and 8 show the associated azimuthal stacks and transfer functions. The parallel stack for the regular fracture spacing case shows a prolonged ringing whereas in the Gaussian distribution case the ringing appears a little more like a series of pulses. However, in both cases the strong ringing of the stack and the transfer function are still present in the direction parallel to the fractures.

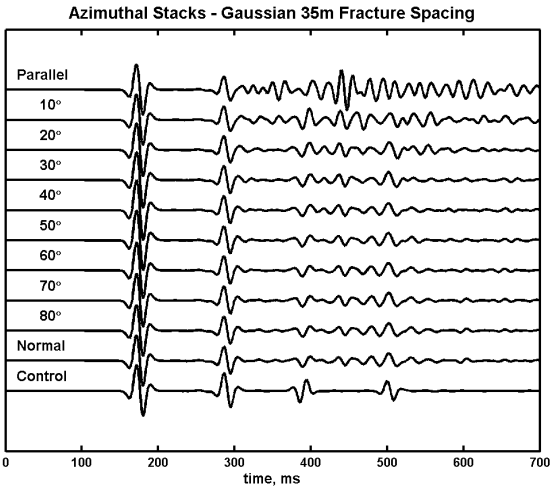

Figure 7. Azimuthal stacks for Gaussian distribution of fractures.

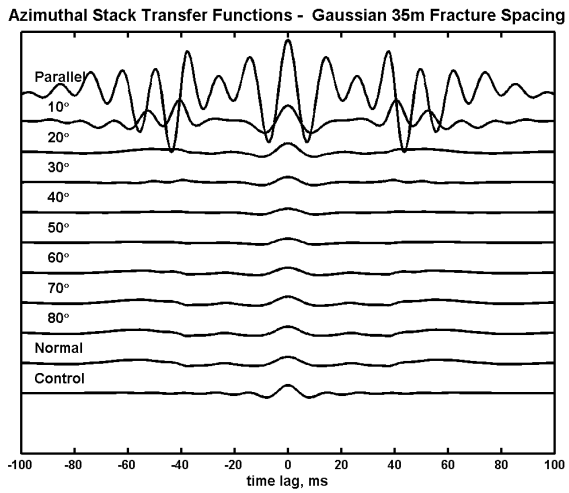

Figure 8. Transfer functions for Gaussian distribution of fractures.

We have chosen only one model to test for the applicability of the methodology in the presence of multiple fractures set. A more thorough analysis will need to be performed since there are many variables to be considered including fracture orientation, spacing, and stiffness. We chose to build a model with two fracture sets. The primary set of fractured is spaced at 35m. The secondary set of fractures is oriented at 45 degrees to the primary set of fractures and spaced 100m apart. Its stiffness was chosen to be 5 times stiffer than the primary set. Figures 9 and 10 show the associated azimuthal stacks and transfer functions. Here it seems that the secondary set of fractures has hardly any affect on the stacks and transfer functions.

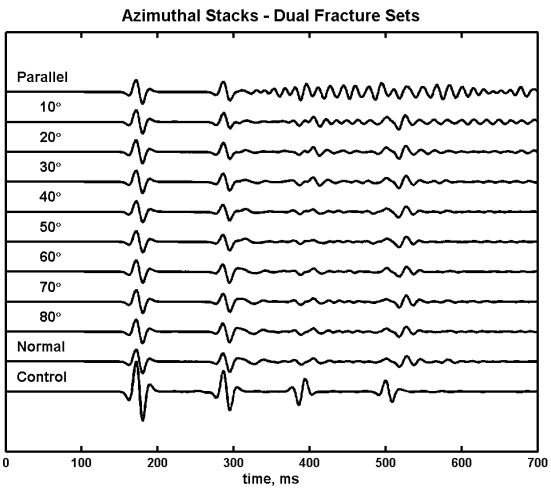

Figure 9. Azimuthal stacks from dual fracture model.

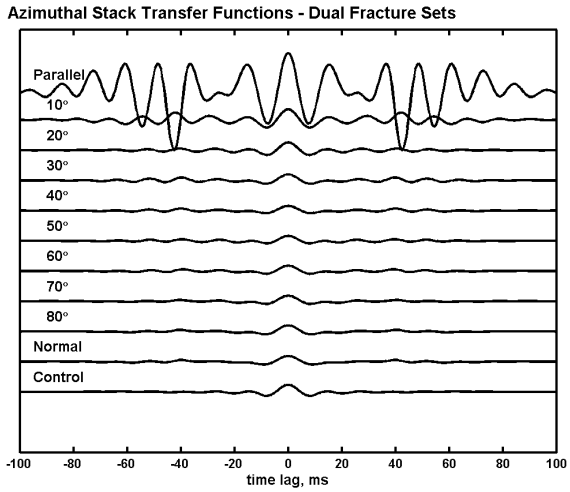

Figure 10. Transfer functions for the dual fracture model.

4. Methodology for Scattering Index

What we have seen so far, is that stacks made in the direction parallel to the primary fractures enhance the ringing scattered energy on the traces. Stacks made in other directions tend to diminish the scattered energy. This same trend is evident on the corresponding transfer functions. Looking more closely the transfer functions for the orientation parallel to fractures, we see clearly their ringiness away from the zero lag. However, in the normal direction the transfer functions are comparatively compact.

In order to quantify the amount of transfer function ringiness or non-compactness, we created a scattering index, SI, defined by:

$$SI = \sum_{i=0}^{m} | t_i | i^n$$

where i is the time lag, t_i is the transfer function (time domain) amplitude at lag i, n is an exponent, typically equal to unity, and m is a lag at which there is no more significant energy in the transfer function. (It is also possible to normalize the scattering index based upon its energy and interval time sample or other such criteria.) The more the transfer function rings, the larger the value of the scattering index. If the transfer function is a simple spike, i.e. representing no scattering, then the scattering index attains a value of zero.

Figure 11 shows the scattering index values for models run with 25, 35, 50 and 100m fracture spacings. These results show that there is a clear maximum of the scattering index in the parallel direction. It is also clear that in the non-parallel directions the scattering index is not zero but fluctuates about a smaller, but fairly consistent value.

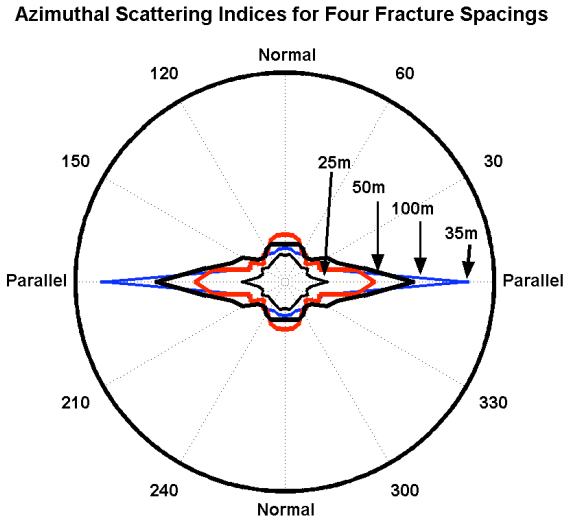

Figure 11: Polar plot of the azimuthal variation of scattering indices derived from the transfer functions of the 25, 35, 50 and 100m fracture spacing models. The scattering index is largest in the direction parallel to the fracture orientation. The largest scattering index is for the 35m fracture spacing, while the smallest shown is for the 25m spacing.

5. Results on field data

In early 2000, a 3D/4C seismic survey was collected over the Emilio Field, located in the central part of the Adriatic Sea, near the eastern coast of Italy. The reservoir unit is a fractured carbonate which from borehole studies suggests the presence of two orthogonal fracture sets oriented ENE and NNW (Angerer et al, 2002). Recent studies have investigated this 3D seismic data using PP and PS wave anisotropy to identify fracture characteristics of the reservoir level (Vetri et al, 2003; Gaiser et al, 2002).

The near to mid range offsets of the preprocessed PP data (Vetri et al, 2003) were stacked in eighteen different azimuthal orientations from East to West using 20 degree wide overlapping ranges. This process created eighteen 3D stacked volumes. The transfer functions and scattering indices for the formation zone were computed for each of these stacked volumes. The scattering indices were sorted and directions for those with the highest ranges of values are plotted in Figure 12, giving a map view of the location and direction of possible fractures determined by this method. Figure 13 shows histogrammed rose plots of the fracture distributions corresponding to the sixteen boxes outlined in green in Figure 12. In several boxes there appears to be no preferred orientation while in many of the boxes the ENE and NNW directions are strongly evident.

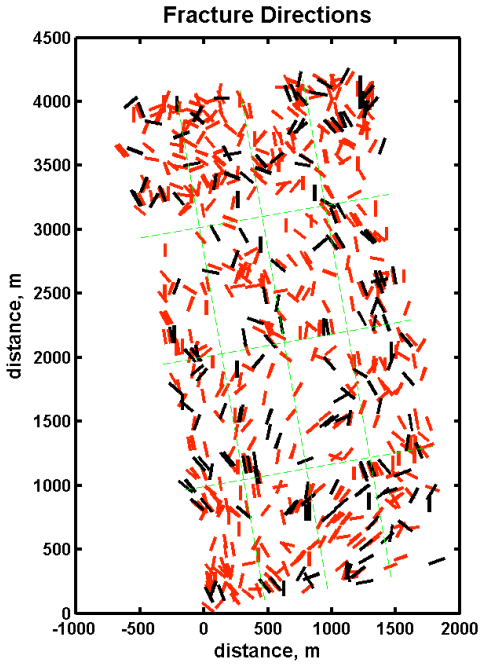

Figure 12. The spatial orientation and distribution of fractures over the Emilio field as indicated from scattering indices of multiple azimuthal stacks. The black and red bars show the orientations for the top two bins of highest scattering indices. The green grid shows the location of the histogram plots in figure 13.

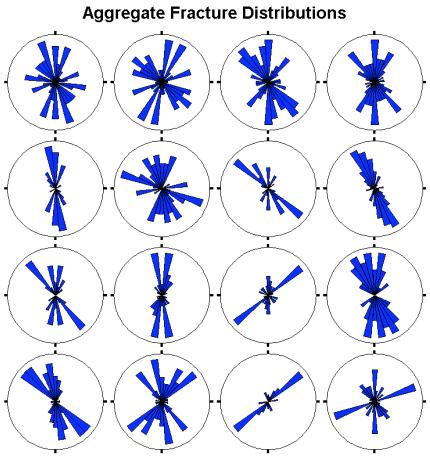

Figure 13. Angular histograms plots of the fracture distributions shown in figure 12. Each plot represents the corresponding subportion of the field cut up by the green dashed lines in Figure 12. The top of each plot represents fractures aligned North.

6. Conclusions

Large-scale zones of fracturing control fluid flow in certain reservoirs, and such zones can scatter seismic energy depending on the fracture density and compliance, as well as the spacing relative to the seismic source wavelength. This scattered wave energy contains information about the fracture properties. Using numerical modeling data we developed a method of analyzing scattered wave energy from fractured reservoirs. A deconvolutional process that measures the 'ringiness' of the transfer function can be used to estimate fracture orientation from azimuthally stacked data. The application of this method on field data provide fracture orientation estimates which generally agree with previous borehole and PS anisotropy studies in the Emilio field.

References

Angerer, E, Horne, S, Gaiser, J., Walters, R., Bagala, S., 2002, Characterization of dipping fractures using Ps mode-converted data, SEG Expanded Abstracts.

Ata, E., and Michelena, R. J., 1995, Mapping distribution of fractures in a reservoir with P-S converted waves, The Leading Edge, v. 12, 664-676.

Gaiser, J., Loinger, E., Lynn, H, and Vetri, L, 2002, Birefringence analysis at the Emilio field for fracture characterization, First Break v 20, 505-514.

Lynn, H., Simon, K. M., and Bates, C. R., 1996, Correlation between P-wave AVOA and S-wave traveltime anisotropy in a naturally fractured gas reservoir, The Leading Edge, v 15, 931-935

Nihei, K.T., et al., 2002, Finite difference modeling of seismic wave interactions with discrete, finite length fractures, 72nd SEG Expanded Abstracts.

Vetri, L., Loinger, E. Gaiser, J. Grandi, A., Lynn, H, 2003, 3D/4C Emilio: Azimuth processing and anisotropy analysis in a fractured carbonate reservoir, The Leading Edge, 675-679.

Willis, M.E., Burns, D.R, Rao, R. and Minsley, B, 2003, Characterization of scattering waves from fractures by estimating the transfer function between reflected events above and below each interval, Annual Sponsors' Meeting of MIT/ERL.

Willis, M.E., Pearce, F, Burns, D.R, Byun, J. and Minsley, B, 2004, Reservoir fracture orientation and density from reflected and scattered seismic energy, EAGE meeting Paris.

Acknowledgements

Our thanks to Lawrence Berkley Lab for use of their 3D finite difference modeling code. We would like to recognize and thank ENI S.p.A. AGIP, the Department of Energy Grant number DE-FC26-02NT15346, and the Earth Resources Laboratory Founding Member Consortium for funding and supporting this work.